Protein dynamics from nuclear magnetic relaxation

Cyril Charlier, Samuel F. Cousin, Fabien Ferrage

Protein Dynamics from Nuclear Magnetic Relaxation

Cyril Charlier, [‡a,b,c] Samuel F. Cousin, [‡a,b,c] Fabien Ferrage,*[a,b,c]

Nuclear magnetic resonance is a ubiquitous spectroscopic tool to explore molecules with atomic resolution. Nuclear magnetic relaxation is intimately connected to molecular motions. Many methods and models have been developed to measure and interpret the characteristic rates of nuclear magnetic relaxation in proteins. These approaches shade light on a rich and diverse range of motions covering timescales from picoseconds to seconds. Here, we introduce some of the basic concepts upon which these approaches are built and provide a series of illustrations.

Key learning points:

- How is nuclear magnetic relaxation linked to molecular motions?
- Which relaxation-based approaches can be used to characterize these motions quantitatively?
- How can chemical reactions at equilibrium be studied with atomic resolution through measurements of magnetic relaxation?
- What are the nature and the time scales of motions that can be studied with this toolkit of relaxation techniques?

1 Nuclear spin relaxation: definitions and physical principles

Most chemists use nuclear magnetic resonance (NMR) daily for the exquisitely precise and quantitative information it provides in the form of frequencies. The proton NMR spectrum of a small molecule displays chemical shifts, from which we learn about the electronic environment, and scalar couplings, which tell us about through-bond connectivities. Once all of this is known, NMR keeps on giving: for instance, the width of an NMR peak contains a wealth of information about motions at the microscopic scale. The aim of this review is first to introduce the underlying principles of the existence of this line width: nuclear magnetic relaxation. Second, we will illustrate the many uses of this phenomenon to access the dynamics of proteins at the atomic scale. Although many basic concepts are introduced in this review, we advise readers who are not familiar with the vector model of NMR to refer to one of the excellent textbooks about NMR, such as ref. 1.[1]

Relaxation can be defined as the irreversible evolution of a spin system toward a steady state, in most cases equilibrium. This evolution is due to fast fluctuations of local magnetic fields exerted on each nucleus. This has two important consequences. First, the scale at which relaxation has to be considered is the level of the atom, which means that relaxation will provide information at the length scale of the atom. Second, relaxation is sensitive to motions at this atomic scale as fluctuations of magnetic fields are due to rotational and translational motions of parts of molecules, whole molecules or of two molecules with respect to each other. Thus, relaxation rates probe molecular motions at the atomic scale.

Relaxation leads to an evolution of a spin system with time and is therefore characterized by a series of rates. The rate that governs the return to equilibrium of the component of the magnetisation that is parallel to the magnetic field, which we will now call longitudinal magnetisation, is called the longitudinal relaxation rate and denoted R_1. The rate of the decay of components of the magnetisation perpendicular to the magnetic field (transverse components) is the transverse relaxation rate, R_2. The line width of NMR signals is directly proportional to R_2. Both rates appear in the fundamental Bloch equation.

Finally, one of the most fruitful aspects of relaxation is cross-relaxation. Cross-relaxation is the relaxation-driven exchange of polarization [polarization is a quantity proportional to the magnetisation divided by the gyromagnetic ratio]. This is the process at the origin of the nuclear Overhauser effect[2] and its ubiquitous use in the nuclear Overhauser spectroscopy (NOESY) experiment.

2 Reorientational dynamics

2.1 Intramolecular orientation-dependent interactions

In the case of biomolecules, relaxation is most often dominated by the fluctuations of strong internal interactions. Figure 1 presents a schematic list of the main internal interactions that contribute to relaxation in proteins. The first interaction is the ubiquitous nuclear dipole/nuclear dipole interaction. Nuclear dipoles abound in biomolecules, such as those of ^{1}H and ^{14}N in natural abundance systems, joined by those of ^{13}C, ^{15}N and ^{2}H in isotopically labelled biomolecules. The strength of the interaction between two nuclear spins I and S is proportional to $\gamma_I\gamma_S/r_{IS}^3$, where γ_I and γ_S are the gyromagnetic ratios of nuclei I and S, and r_{IS} is the distance between the two nuclei. Most protons within a 5 Å distance of another proton contribute to its relaxation. All other nuclei have smaller gyromagnetic ratios, so that only protons within one to two bonds of another nucleus (^{13}C, ^{14}N, ^{15}N, and ^{2}H) should be considered and only dipolar couplings between the nuclei of directly bound ^{13}C, ^{14}N, ^{15}N, and ^{2}H atoms have significant contributions to relaxation.

The shielding of the magnetic field by electrons depends on the orientations of molecular orbitals with respect to the magnetic field. The fluctuating part of this interaction is the chemical shift anisotropy (Fig. 1.b). This interaction is directly proportional to the magnetic field. It is weak at low magnetic fields but becomes the predominant mechanism of relaxation at the highest magnetic fields accessible today (*ca.* 20 T) for most spins ½ nuclei in an sp2 environment (*e.g.* amide ^{15}N,

carbonyl and aromatic ^{13}C), as shown in Figure 2 a,d.

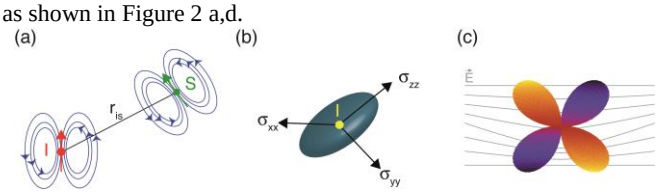

Figure 1: Schematic representation of the main interactions contributing to relaxation in biomolecules. (a) Dipole-dipole interaction, either between two nuclei or a nucleus and an electron, the magnetic field lines of the dipoles I and S are shown. (b) Chemical shift anisotropy, we represent a graphical representation of the components of the chemical shift tensor σ_{xx}, σ_{yy}, and σ_{zz}. (c) Quadrupolar coupling: we show a schematic representation of the nucleus electric quadrupole interacting with the electric field gradient.

The magnetic dipole of the electron is three orders of magnitude (658 times exactly) larger than that of the proton. Hence, the dipole-dipole interaction between a nucleus and an electron (also known as the hyperfine interaction) will dominate all relaxation processes if any unpaired electron lies in the vicinity of a nucleus. With high-spin systems, this interaction can dominate relaxation at distances up to ~20 Å from the metal ion.

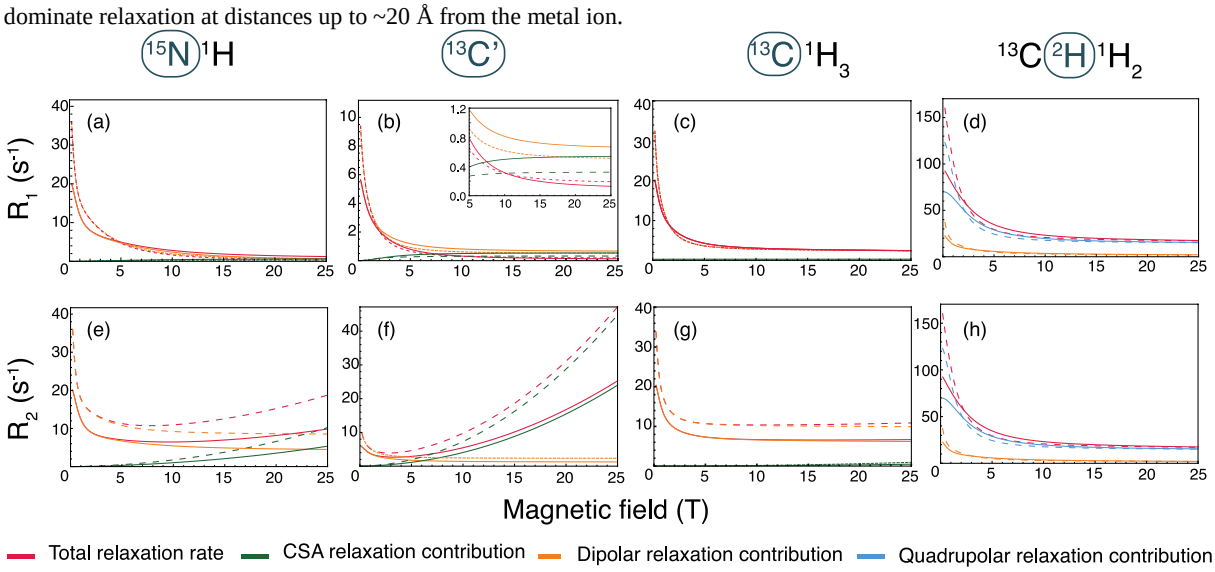

Figure 2: Relaxation rates as a function of the magnetic field in a few representative groups: (a) the backbone amid ^{15}N; (b) methyl group ^{13}C; (c) methyl group ^{2}H; and (d) backbone carbonyl ^{13}C. Total relaxations are display in red, whereas the CSA, dipolar and quadrupolar contributions are shown respectively in green, yellow, and blue. Theses calculations were carried out for typical rigid groups in proteins with an overall correlation time τ_c = 5 ns (10 ns) for plain (dashed) line. Details of the parameters used are given as supporting information.

Finally, nuclei with a spin number larger than 1/2 (such as ^{14}N and ^{2}H) possess a non-vanishing electric quadrupole, which interacts with the electric field gradient of the electrons. This interaction is often strong and the dominant mechanism of relaxation in nuclei with spins larger than 1/2. The moderate quadrupolar interaction in deuterons makes it amenable to quantitative measurements of relaxation.[3] With this exception, fast relaxation of nuclei with quadrupolar interactions explains why liquid-state biomolecular NMR exclusively focuses on spin 1/2 nuclei.

2.2 Correlation functions and spectral density

Most liquid-state NMR experiments are carried out in isotropic phases: for all conformations of a molecule, all orientations in the laboratory frame are equally probable. The transition between these orientations is very fast: it takes a few picoseconds for water molecules to reorient in solution and a few nanoseconds to a few tens of nanoseconds for proteins. [as a rule of thumb, at room temperature, the overall rotational correlation time of a protein in ns is approximately half of its molecular mass in kDa. For instance, the protein ubiquitin, with a molecular mass M ~ 8 kDa has a rotational correlation time of ~4 ns at 25º C].

First and foremost, this fast rotation leads to the averaging of all above-mentioned orientation-dependent interactions. Hence, liquid-state NMR spectra often consist of a series of sharp lines. However, rotational motions lead to fluctuations of these interactions on picosecond to nanosecond timescales. These fluctuations have an important effect on nuclear spins: relaxation.

We can, for instance, consider a pair of dipolar-coupled spins 1/2 in a given molecule. Let us consider the evolution of a transverse magnetisation under the longitudinal part of the magnetic field produced by the neighbouring dipole (i.e. the dipolar interaction). When we consider a time t that is shorter than the typical timescale of the reorientation of the molecule □, the dipolar interaction has seldom changed as compared to the time t = 0. The magnetisation of nuclear spins continues to evolve in a way similar to the evolution initiated at time t = 0. When the time t is much larger than □, the orientations of the molecule at times t and t = 0 are uncorrelated and the evolution of the magnetisation under the dipolar interaction is no longer

efficient. For each molecule with a different orientation, the evolution of the magnetisation will be different. Hence, in an ensemble with equal probability for all orientations, the effect of the dipolar interaction during an effective interval will lead to a decay of the ensemble average of the magnetisation. This is transverse relaxation. The longer the time the longer the evolution under the dipolar interaction is efficient and the faster is transverse relaxation (and the larger the line width). Indeed, transverse relaxation rates in proteins are nearly proportional to the molecular mass of a protein. Impracticably large line widths limit the application of traditional NMR techniques to non-deuterated protein of about 50 kDa.

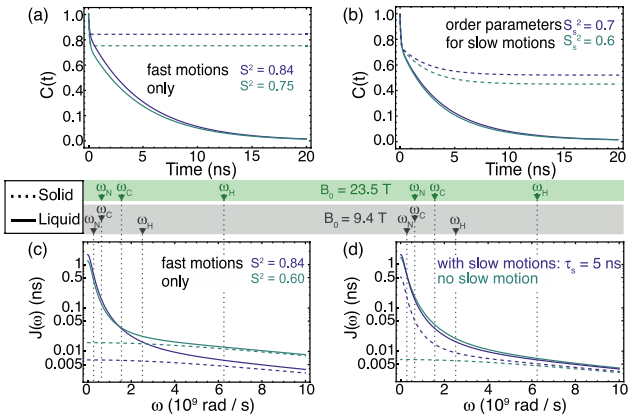

Figure 3: Influence of the amplitudes and timescales of internal motions on the correlation functions C(t) (a,b) and spectral density functions J(ω) (c,d) found in solids and liquids. (a,b) Influence of the amplitude of internal motions on the correlation function in solids (dashed lines) and isotropic liquids (solid lines) for (a) fast motions and (b) nanosecond motions with a correlation time similar to the one of overall tumbling (here the overall correlation time is τ_c = 5 ns). (c,d) Influence of the amplitude of internal motions on the spectral density function in solids (dashed lines) and isotropic liquids (solid lines) for (c) fast motions and (d) nanosecond motions with a correlation time similar to the one of overall tumbling. (c,d) The resonance frequencies of nitrogen-15, ω_N , carbon-13, ω_C, and proton, ω_H, are shown for magnetic fields of 9.4 T (400 MHz spectrometer) in green and 23.5 T (1 GHz spectrometer) in grey to illustrate which values of the spectral density function typically contribute to relaxation. Details of the correlation functions and spectral density functions are given as supporting information.

Fluctuations of the transverse components of the dipole magnetic field have a similar effect. However, one should keep in mind that the transverse part of the magnetisation follows a precession under the interaction with the B_0 magnetic field at the Larmor frequency [the Larmor frequency is the resonance frequency of a nucleus. It is an angular frequency $\omega_0 = -\gamma B_0$; where γ is the gyromagnetic ratio of the nucleus and B_0 the external magnetic field]. Hence, only the fluctuations at the Larmor frequency are efficient. Only transverse components of the magnetic field lead to an evolution of a longitudinal magnetisation. Longitudinal relaxation occurs under the fluctuations of interactions at the Larmor frequency.

A quantitative description of the process presented above involves the introduction of two functions. (1) The correlation function for the reorientation of the vector that links the two coupled nuclei. Such correlation functions are represented in Figures 3.a-b. (2) The Fourier transform of the correlation function is the spectral density function, represented in Figure 3.c,d. Slow fluctuations of the longitudinal magnetic field to transverse relaxation contribute to the value of the spectral density at zero frequency, J(0). Fast fluctuations of the transverse magnetic field contribute to the values $J(\omega_0)$, where ω_0 is the Larmor frequency of the nucleus.

For the sake of consistency, we have only described the effect of a dipole-dipole interaction on relaxation. Similarly, the fluctuations of chemical shifts and quadrupolar couplings under the reorientation of a molecule lead to relaxation in an analogous way.

2.3 Models of motion

We have, so far, introduced important concepts about the relaxation of nuclear spins. We will now discuss in more detail the nature of reorientational motions that give rise to relaxation via fluctuations of internal interactions. Many types of motions occur in proteins. In this section, we will list the most important motions and present a few models used for the interpretation of relaxation rates in terms of motions. The dominant motion that occurs in a well-folded single domain protein is the rotational diffusion of the entire domain, which is usually referred to as the overall or global motion. The study of the overall motions is informative on the hydrodynamics of a protein. In multi-domain proteins, motions of domains relative to each other are usually allowed and can have wide amplitude. We refer to these as domain motions. Within a protein domain, loops and turns can wobble on fast nanosecond time scales that can be probed by relaxation.

Some conformational transitions involve a reorganisation of some interactions such as hydrogen bonds or salt bridges and the passage through a significant energy barrier. These transitions take place on time scales ranging from the hundreds of nanoseconds to seconds. They will be discussed in sections 4 and 5. The transition between side chain rotamers is often allowed on fast nanosecond and hundred of picosecond time scales. The fastest motions are vibrations and librations of the protein backbone and side-chain, which also lead to measurable contributions to the reorientation of groups of atoms both in the side chains and the backbone of a protein. Such motions are variable in time scale and amplitude and depend on the local

pattern of intramolecular interactions.

[In disordered proteins, rotational diffusion of segments of the protein is also allowed, such segments can be transiently folded small domains or a group of consecutive residues of a length comparable to the persistence length. With a persistence length of about seven residues, there is no physical reason to observe overall rotational diffusion in a disordered protein. The separation of the timescales of segmental (translation and rotational) diffusion and conformational transitions, or their interplay, is an active field of research.]

A core assumption of most analysis of relaxation in proteins is the decoupling of the overall motion and internal motions. Thus, the overall motion of a single-domain protein is described with the usual concepts of hydrodynamics for isotropic, axially symmetric or fully asymmetric rotational diffusion. Local motions can be represented by physical models, such as diffusion in a cone or anomalous diffusion in a rugged potential.[4] Other approaches voluntarily avoid the use of physical models of local motions and rely on effective parameters. The most popular approach for the interpretation of relaxation in proteins falls in this category. The model-free approach[5] relies on two parameters: an order parameter S^2, which describes the amplitude of motions (full disorder for $S^2 = 0$ and complete rigidity for $S^2 = 1$) and an effective correlation time for these local motions. One should keep in mind that the "model-free" approach is indeed free of a precise physical model to describe the nature of the internal motion[5,6] but not free of any model or hypothesis. Another similar approach is the Gaussian axial fluctuations (GAF)[7] model of internal motions, which was inspired by the analysis of motions in molecular dynamics simulations. The GAF model describes motions of the peptide plane in proteins with fluctuations of orientation angles around principal axes (the main axis is almost aligned to the $C_{\alpha i-1}$-$C_{\alpha i}$), with a Gaussian amplitude. This model assigns different amplitudes for motions around different axes but not different correlation times (or rotational diffusion coefficients).

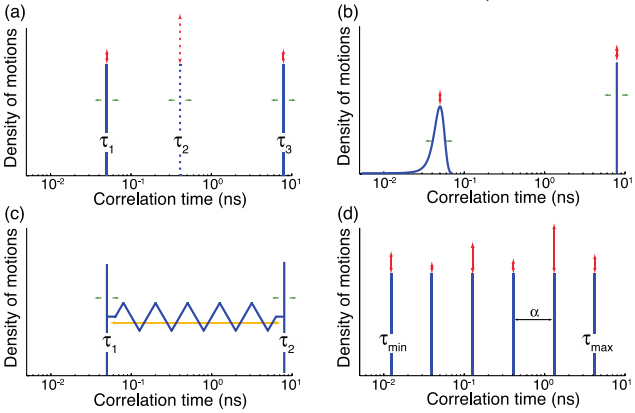

Figure 4: Distribution of correlation times for a series of models of motions in proteins studied by NMR. In the (a) Model-Free[5] (two correlation times) and Extended Model-Free[8] (three correlation times) approaches: the value and the relative weight of each correlation time can be fitted to experimental data. (b) A broad and continuous distribution of local motions can be introduced.[4, 9] (c) SRLS approach[10] for which local and overall motions, with adjustable correlation times are coupled by a local potential. (d) A model-free reconstruction of the distribution of correlation times can be obtained by regularization, such as IMPACT:[11] the values of the distribution of correlation times can be evaluated at a series of fixed positions, equally spaced on the logarithmic scale.

The statistical independence of overall and local motions has been challenged in folded proteins, bringing significant differences in the quantitative description of loop and domain motions. The slowly relaxing local structure model (SRLS) describes local motions as diffusion in a potential imposed by the molecular environment.[10] Rotational diffusive motion of the local entity (peptide plane, loop or domain) and the overall macromolecule become coupled. The general framework of description of reorientational motions in proteins has to be rethought when there is no well-defined structure, such as in intrinsically disordered proteins. In this case, the absence of domains mostly rigid on the timescale of rotational diffusion prevents the definition of an overall diffusion tensor. So far, the analysis of relaxation rates in disordered proteins has focused on the description of local distribution of correlation times.[12] Figure 4.d shows that such a distribution can be reconstructed in a model-free manner with regularization methods.[11]

2.4 High-field measurements of relaxation

High-field relaxation parameters contain information about the overall rotational diffusion and internal dynamics in biomolecules. Typically, extraction of this information follows two approaches. In the first case, the form of the spectral density function is assumed and so the extraction is straightforward. The most popular frameworks to derive the parameters of local dynamics from a set of ^{15}N relaxation data for backbone motions (or ^{2}H relaxation rates in methyl groups) are the model-free and extended model-free approaches.[5, 8] In general a model selection step based on statistical significance is performed to choose the appropriate functional form of the spectral density function.[13] Note that complex models of motions[8] are more likely to be statistically significant if a large number of experimental data points is used. Relaxation rates measured at multiple magnetic fields are often required to use the extended model-free description.

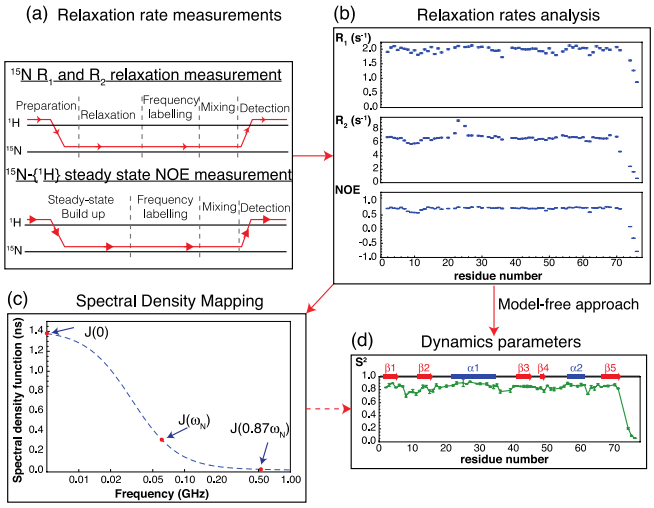

Figure 5: High-field relaxation measurements analysis. (a) Principle of the ^{15}N R_1 , ^{15}N R_2 and ^{15}N-{^{1}H} NOE measurements. (b) ^{15}N R_1, ^{15}N R_2 and ^{15}N-{^{1}H} NOE (Ubiquitin, 14.1 T).[17] (c) Spectral density mapping to derive values of the spectral density function at a few characteristic frequencies ($J(0)$, $J(\omega_N)$ and $J(0.87\omega_H)$).[16] (d) Order parameters obtained from the fit to the spectral density mapping results (c) or from a direct fit to measured relaxation rates (b) using the model-free approach.

The second approach relies on a minimal set of assumptions on the functional form of the spectral density function and underlying model. The spectral density mapping method[14] is based on the inversion of the set of equations for R_1, R_2 and NOE rates expressed as linear combination of $J(\omega)$ at 0, ω_H, ω_N, $\omega_H \pm \omega_N$ frequencies in the relaxation theory.[15] This method is general, irrespective of the overall diffusion properties and applicable to folded domains, multi-domain or disordered proteins. Its reduced version based on a limited set of relaxation rates[16] is straightforward to implement. However, the values of the spectral density function at a few frequencies represent a dataset difficult to interpret. The first approach, which provides most often local order parameters, is usually preferred when applicable.

The approach is illustrated in Figure 5 for backbone nitrogen-15 relaxation. It is similarly applied to carbon-13 or deuterium relaxation in methyl groups. High-field relaxation samples a limited range of the spectral density function (see Figure 3). The philosophy of high-field relaxation approaches is to obtain data of high precision and accuracy so that slight variations due to small amplitude motions can still be quantified. However, approaches with extensive sampling of the spectral density function should be favoured when motions on several orders of magnitude of correlation times are to be characterized.

2.5 Relaxometry

Relaxometry is the measurement of relaxation rates over a broad range of magnetic fields. The most popular approach to relaxometry is called fast field-cycling relaxometry.[18] In this approach, the initial polarization is carried out at a first magnetic field B_{pol}, which is then switched rapidly (within milliseconds) to a relaxation field B_{rel} (Figure 6.a). Finally, the magnetic field is switched to the observation field B_{obs}. Such fast field changes are possible with the use of electromagnets. However, all fields are below 2 T, with the exception of some hybrid systems where magnetic fields up to 3 T can be reached. Clearly, such limited magnetic field and magnetic field homogeneity preclude the measurement of high-resolution spectra of proteins. In general, the overall signal intensity is recorded as a function of relaxation delay. The site-specific nature of the measurements is lost.

On the other hand, the range of magnetic fields accessible is spectacular. Magnetic fields from a few μT (below the Earth magnetic field) up to 1 T are readily accessible. This corresponds to a proton frequency sampling up to 42 MHz and down to a few kHz (reliable measurements below a few tens of μT are challenging). The corresponding reciprocal correlation times are thus in the range:

$$\tau_{min} = \frac{1}{\gamma B_{rel}^{max}} < \tau_c < \tau_{max} = \frac{1}{\gamma B_{rel}^{min}} \qquad (1)$$

For protons, with B_{rel}^{max} = 1 T and B_{rel}^{min} = 0.1 mT, we obtain τ_{min} = 3.7 ns and τ_{max} = 37 μs. For deuterium, we obtain: τ_{min} = 24 ns and τ_{max} = 240 μs. These correlation times span four orders of magnitude and mostly exceed by far the typical correlation times of overall diffusion of proteins amenable to solution-state NMR studies. Thus applications to proteins in solution have focused on the identification of correlation times in the low nanosecond range, in particular signs of aggregation and the presence of slow motional modes in disordered proteins.[19]

The most unique information from such relaxometry approaches can be obtained when overall rotational diffusion is hindered. In the absence of overall rotational diffusion, slower dynamic processes with timescales up to 100 μs can be probed. Relaxometry has been applied successfully to proteins in powders[20] or proteins in solution immobilized by cross-linking.[21] Although the direct observation of protein proton relaxation is possible, the description of field-dependent

relaxation of water protons, deuterons or oxygen-17 nuclei is very informative. Water molecules bound in internal sites within a protein experience a dramatic reduction of motions. Water access to and release from internal sites requires extensive protein motions, which can thus be probed indirectly. The dynamics of exchange of water molecules between the solution and internal binding sites gives rise to variations of longitudinal relaxation rates. Exchange processes as fast as 20 ns and as slow as a few microseconds have been identified in BPTI, for instance.[21]

2.6 High-resolution relaxometry

The characterization of relaxation rates over a broad range of magnetic fields allowed by relaxometry comes with a price: the loss of high-resolution observation precludes in most cases the ability to obtain site-specific information. High-resolution can be recovered if the observation field B_{obs} is high enough and very homogeneous. In short, high-resolution relaxometry is possible if the observation is performed in the high-field magnet of an NMR spectrometer. The broad range of low magnetic fields B_{rel} for relaxation is effortlessly obtained as the stray field of the superconducting magnet. Transition from B_{rel} and B_{obs} is achieved by displacing the sample (or the probe containing the sample) to a chosen position of the stray field (Figure 6.b).[22] This motion is slower than the induction times of electromagnets. Thus transitions between high and low fields can take 30 to 100 ms, which limits the range of accessible relaxation rates.

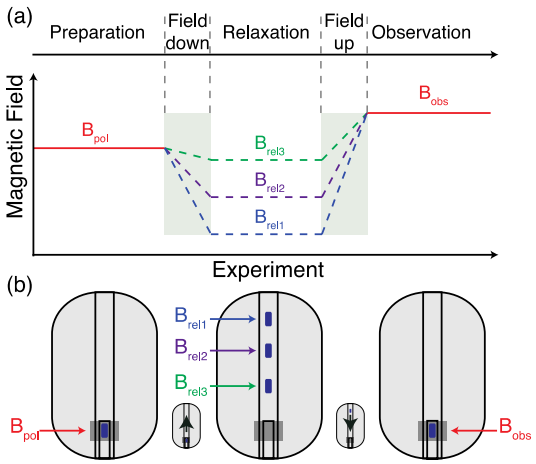

Figure 6: (a) Principle of relaxometry. (b) Principle of high-resolution relaxometry: the magnetic field is changed by moving the sample from the magnetic centre of a commercial magnet to a chosen position of the stray field. The experiment is similar to (a) but the polarization and observation fields are identical.

The observation of the signal is performed with a liquid-state NMR probe on a solution-state sample. As mentioned above, this limits the range of accessible correlation times to values below or near the correlation time for rotational diffusion of the entire protein. So far, high-resolution relaxometry has been applied to two proteins.[17, 23] Backbone nitrogen-15 relaxation rates have been measured at several high fields and at low fields down to 0.5 T. In these two studies, motions on low-nanosecond timescales (about 0.8 and 2 ns) have been identified in small subdomains: a β-hairpin of the SARS nucleocapsid protein[23] and the β1-β2 turn of human ubiquitin.[17]

2.7 Relaxation in the solid state

We saw above that overall rotational diffusion was key to observe sharp signals in solution state NMR, as it led to the fast averaging of orientation-dependent interactions (dipolar coupling, chemical shift anisotropy, quadrupolar coupling). On the other hand, overall rotational diffusion is a major limitation for studies of motions in proteins in solution. Internal reorientational motions significantly slower than a few tens of ns can only be explored with immobilized proteins.

Modern solid-state NMR can solve this dilemma. Fast rotation of a solid sample around an axis that is positioned at the so-called magic angle (54.7°) with respect to the magnetic field allows for a complete averaging of orientation-dependent interactions such as dipolar couplings, chemical shift anisotropy and quadrupolar couplings. Magic angle spinning solid-state NMR (MAS-ssNMR) provides high-resolution spectra of immobilized proteins, within micro-crystals, native oligomers, membranes, sediments or precipitates.

As can be seen in Figure 3, only internal rotational motions lead to fluctuations of orientation-dependent interactions in solids. In principle, there is no longer an upper limit to the correlation times of processes that can be characterized by relaxation in solids. However, motions in the microsecond range are expected to lead to relaxation rates so high that experimental measurements would become challenging.

The approach followed in relaxation studies of solid-state protein samples resembles closely the methods developed for high-field relaxation of solution-state samples (see section 2.4). Longitudinal relaxation rates of nitrogen-15 or carbon-13 nuclei can be measured with good accuracy. The spectral density at very low frequency is derived from measurements of relaxation rates in the rotating frame, called $R_1\rho$ (see section 5.4). Relaxation can become inefficient and relaxation times can exceed

several seconds for rigid systems with restricted fluctuations of orientation-dependent interactions (*e.g.* a rigid single domain protein in a microcrystal). This becomes a clear limitation, as the experimental time necessary to record relaxation decays of the most rigid residues is impractically long and the measurement of such small rates becomes vulnerable to artefacts.
Large datasets have been recorded in some microcrystalline model systems[24] and it has been shown that nanosecond timescale motions could be quantified. In the particular case of microcrystalline samples, non-native intermolecular contacts may hinder large collective motions. Thus the amplitude of motions can be smaller than what is measured in solution-state studies even though motions over a wider range of correlation times are probed in solids.
Solid-state protein samples are not as dramatically altered by temperature as solution-state samples. In particular, such systems are immune to freezing to some level. This has empowered studies of protein dynamics from relaxation over unprecedented ranges of temperatures, for instance from 277 down to 110 K.[25] The exploration of such a broad temperature range allows for the selective activation of motions as a function of their activation energies and a description of the conformational energy landscape of a protein with unprecedented detail (see Figure 11).

3 Translational dynamics

In the case of small molecules, water, or any small organic molecule in a deuterated organic solvent, a significant, sometimes dominant, contribution to relaxation is the fluctuation of nucleus-electrons dipolar interactions. Molecules with non-zero electronic spin include molecular dioxygen dissolved in the solvent and ions of d-elements that exist as impurities in the solution. Such a relaxation process is well known and understood.[26]
Relaxation is typically much faster in proteins than in small molecules so that such contributions to relaxation are usually negligible. However, minute translational motions are important when we consider fluctuations of the distance between two dipoles on timescales that are relevant to relaxation (ps-ns). If the interaction between two nuclear dipoles is considered, one should keep in mind that the distance between the two nuclei should be very small (a few angstroms at most). Translational and reorientational motions are very difficult to disentangle on such short length-scale.
The presence of a paramagnetic centre contributes to nuclear spin relaxation owing to the dipolar interaction between the unpaired electron(s) and the nucleus. A paramagnetic center is naturally present in metalloproteins or chemically attached via the thiol function of a surface-exposed cysteine. The observed paramagnetic relaxation enhancement (PRE) is roughly proportional to r_{eN}^{-6}, where r_{eN} is the average distance between the nucleus and the paramagnetic centre. PRE's can be detected for electron-nucleus distance up to ~30 Å due to the large magnetic moment of the unpaired electron(s). In some cases translation dominates and relaxation can be used to characterize such motions.
A conventional approach to determine PRE rates consists in a comparison of signal intensities on ^{15}N-^{1}H HSQC spectra in paramagnetic and diamagnetic (for instance a nitroxide paramagnetic probe can be reduced) states. PRE effects are conventionally measured by the intensity ratios (I^{para}/I^{dia}). Other approaches have been developed by considering the ratio of peak volumes or by measuring directly the transverse relaxation R_2 in para- and diamagnetic states.[27]

3.1 Intramolecular translational diffusion

Translational motions are restricted in the rigid secondary structure elements of well-folded proteins. However, flexible loops undergo significant translation motions, similarly one may describe the exploration of the conformational space in disordered proteins as translations of parts of the polypeptide chain. Chemical bond vibrations are small, pm-scale translations, which are ubiquitous in all molecules. In our case, such small motions are innocuous to long-range interactions; however, they can alter significantly effective dipolar couplings between the nuclei of the two atoms involved in the chemical bond. These motions are fast, on low ps to high fs timescales, and rather uniform. For instance, few variations of these motions will be observed in between two different N-H^N pairs in a protein.
In a disordered protein, the relative motions of two points (e.g. a nucleus and a paramagnetic chemical group) taken along the protein chain can be described as a combination of translation (the distance varies) and rotation (the orientation of the vector between the two points varies). When the electron spin and the nuclear spin are close, motions lead to more reorientation than fluctuation of the distance. When the two spins are far, the contribution of small motions to reorientation becomes negligible and fluctuations can be best described by translation diffusion in a potential. Characteristic segmental diffusion times have been found to range between 1 and 3 ns in an unfolded protein.[28] Paramagnetic relaxation enhancements are also used as probes of so-called "long-range contacts", which is somehow an oxymoron, but designates transient contacts between regions of a protein significantly separated in the primary sequence. In that case, PRE's are due to contacts between areas of the protein that are more prevalent than expected from a random fully disordered polymer. Such contacts are often mediated by electrostatic or hydrophobic interactions and demonstrate the existence of compact states of disordered proteins.[29]

3.2 Highlighting transient proximity.

Transient contacts are not a marker of disordered proteins but an intrinsic feature of conformational landscapes of isolated proteins and of the mechanisms of their interactions. PRE's have been employed to study a wide range of systems, from weakly populated states to transient interactions, such as encounter complexes, or specific protein-protein or protein-DNA interactions, see [27] and references therein. The initial step of forming a protein-protein interface typically begins with a non-stable "encounter complex". PRE's have been used to detect the presence of weakly populated encounter complexes in a fast exchange regime.[27, 30]

PRE's can also be used to explore different states of multi-domain proteins where the internal rearrangement can be crucial for their multiple biological functions. More recently, PRE experiments have been used to identify "invisible states" characterized by a short distance between nuclei and a paramagnetic probe. The $\langle r^{-6} \rangle$ dependence of PRE rates leads to exquisite sensitivity to such weakly populated transient states.[27]

The presence of many interconverting conformations in IDPs limits the use of classical techniques to determine interatomic distances. To refine the conformational ensemble of IDPs, PREs are used to determine long-range distances.[31] Sophisticated data analysis has then to be used to refine the conformational space of an IDP.[29]

4 Chemical exchange

4.1 Defining chemical exchange

Most biomolecular systems are in a stable dynamic equilibrium in an NMR sample. Such dynamic equilibrium includes proton exchange with the solvent for acidic and basic moieties, conversion between conformational states, exchange between a free form and a state bound to an ion, a small ligand, or another biological macromolecule. In such a dynamic equilibrium, some nuclei may experience two or more chemical environments (*i.e.* two or more chemical shifts) in the course of an NMR observation. This phenomenon is called chemical exchange. The effect of chemical exchange on NMR spectra and apparent relaxation rates can be best explained in the case of a two-site exchange (Scheme 1 and Figure 7).

	$A \underset{k_{B\to A}}{\overset{k_{A\to B}}{\rightleftharpoons}} B$		$k_{ex} = k_{A\to B} + k_{B\to A}$
population	p_A	p_B	$p_A + p_B = 1$
chemical shift	δ_A	δ_B	$\Delta\delta_{AB} = \delta_B - \delta_A$
precession frequency	ω_A	ω_B	$\Delta\omega_{AB} = \omega_B - \omega_A$

Scheme 1. Parameters of two-site exchange.

The regime of chemical exchange is defined by the comparison of the kinetic constant of the exchange process and the difference of chemical shifts between the two sites measured as an angular frequency $\Delta\omega_{AB}$. Two extreme cases can be identified: when the exchange is slow $k_{ex} << \Delta\omega_{AB}$, the signals of the two exchanging species can be observed (k_{ex} is the sum of the effective first order forward and backward rates for the reaction: $k_{ex} = k_{A\to B} + k_{B\to A}$); this regime is called slow exchange. When the rate of exchange is high $k_{ex} >> \Delta\omega_{AB}$, a single signal at the population-weighted average chemical shift can be observed: this is called fast exchange. The frontier between the two regimes is called coalescence: the two peaks merge to form an extremely broad signal. Coalescence happens when the rate of exchange k_{ex} is close to the difference in chemical shift between the two sites measured as an angular frequency $\Delta\omega_{AB}$: $k_{ex} \sim \Delta\omega_{AB}$. Note that, in the case of skewed populations (Figure 7.i-m), the weaker peak is also the broader one. Thus, the observation of a single peak in an exchanging system is not a certain indication of the presence of fast exchange, as the peak of a minor state can be broadened beyond detection. Such weakly populated excited states in slow exchange are often called "invisible states".[32]

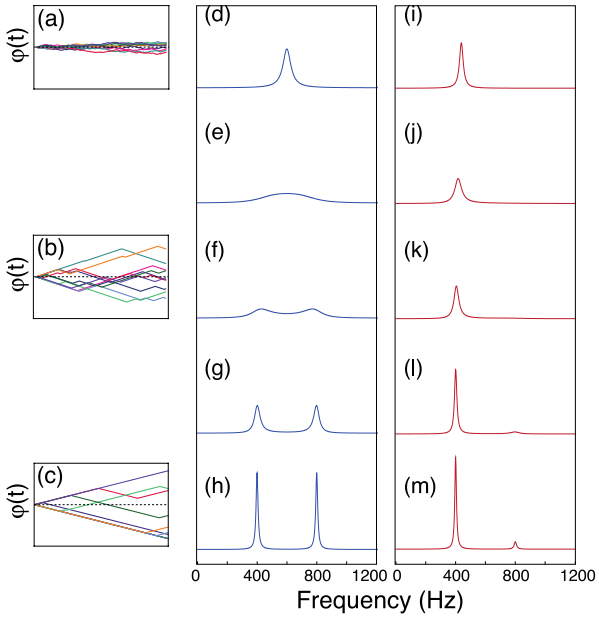

Figure 7: Illustration of the effect of chemical exchange for two-site exchange. (a-c) effect of exchange on the phase of precessing magnetisation in the case of (a) fast, (b) intermediate and (c) slow exchange. The dispersion of the phase of magnetisation in the intermediate case leads to enhanced transverse relaxation rates. (d-m) Effect of two-site chemical exchange on NMR spectra. (d)-(h) $p_A = p_B = 0.5$ and in

(i)-(m) $p_A = 0.1$ and $p_B = 0.9$. Calculations were performed for values of the exchange rate k_{ex}: (d, i) 10000 s^{-1}, (e, j) 2000 s^{-1}, (f, k) 900 s^{-1}, (g, l) 200 s^{-1}, (h, m) 20 s^{-1}; the difference of chemical shifts between exchanging sites corresponds to a frequency $\Delta\omega_{AB}/2\pi = 400$ Hz.

Although chemical exchange can be quantified by a direct analysis of line shapes, a series of techniques has been developed over the years to obtain quantitative information of high value: the kinetics of the exchange process (the exchange rate), the thermodynamics (the populations of states), and structure (the chemical shift of exchanging states). In the case of two-site fast exchange, the contribution of chemical exchange to relaxation R_{ex} is:

$$R_{ex} = \frac{p_A p_B \Delta\omega_{AB}^2}{k_{A\to B} + k_{B\to A}} \qquad (2)$$

where p_A and p_B are the populations of exchanging sites A and B; $\Delta\omega_{AB}$ is the difference of chemical shift in rad.s^{-1}; $k_{A\to B}$ and $k_{B\to A}$ are the rates of the (effective) first order reaction. This simple expression shows how chemical-exchange-induced relaxation is rich in information on thermodynamics (p_A and p_B), kinetics ($k_{A\to B}$ and $k_{B\to A}$), and chemical structure ($\Delta\omega_{AB}$).

4.2 Chemical reactions at equilibrium: the example of proton exchange

Most NMR studies are performed on chemical and biochemical systems that are, in principle, at equilibrium. Fast precipitation of a protein sample sometimes bitterly reminds us that a good sample is actually out of equilibrium. However, in many cases, sample degradation occurs on much slower timescales (days to years) than chemical processes in the sample.

An obvious set of chemical reactions that take place in any protein sample is proton exchange between the solvent (water molecules, hydroxyl and hydronium ions) and acidic and basic groups, such as carboxyl groups of aspartic and glutamic acid, or ammonium groups at lysine side chains. Several techniques have been developed to study proton exchange kinetics.[33] Proton exchange is a fast chemical process so that the effect on the spectrum of neighbouring nuclei is usually in the fast exchange regime. Thus, a population average chemical shift between those of the acidic and the basic states is observed. Such an observation has been used to titrate individual carboxyl or lysine groups in proteins and determine site-specific pK_a.[34, 35]

Recently, the kinetics of proton exchange in individual carboxyl groups in a protein have been measured in a simple way: the contributions of exchange between the acidic and basic states to the transverse relaxation rates of the carboxyl carbon-13 nuclei have been measured as a function of pH. The spectra collected during this pH titration provide the difference of chemical shifts between the two states as well as the equilibrium constant. Transverse relaxation rates then provided the kinetic rates (see equation 2). Site specific first order rates for the deprotonation reaction up to 3×10^6 s^{-1} and bimolecular protonation rates up to 3×10^{11} $s^{-1}M^{-1}$ could be measured.[36]

4.3 Conformational dynamics

Many exchange processes that are amenable to NMR studies do not involve the breaking of covalent bonds but rather involve the reconfiguration of many weaker interactions such as salt bridges, hydrogen bonds, and van der Waals interactions. Such processes correspond to small- or large-scale conformational transitions in a protein. This transition can occur between two or more compact conformations, between a well-folded state and partially unfolded states. It can also be induced by ion/ligand binding or the interaction with another biological macromolecule. The study of conformational dynamics is a lively and exciting area of research in biomolecular NMR and methods to study these motions will be presented in the following section.

5 Methods for chemical exchange

Over the past several decades, many methodological contributions have built a complete toolbox for the characterization of μs to s time scale motions in biomolecules. This has been made possible by the quantification and control of chemical exchange contributions to relaxation. In this section, we will present briefly the most commonly used methods to quantify such exchange processes ranked in increasing order of the rate of exchange for which they are appropriate: exchange spectroscopy (k_{ex} rates ~10^0 to ~10^2 s^{-1}); chemical exchange induced saturation transfer (k_{ex} rates ~10^1 to ~10^3 s^{-1}); Carr-Purcell-Meiboom-Gill (CPMG) relaxation dispersion (k_{ex} rates ~10^2 to ~10^3 s^{-1}); and relaxation in the rotating frame (k_{ex} rates ~10^3 to ~10^5 s^{-1}).

The theoretical framework and mathematical expressions to be used in the analysis of such experiments are reviewed in detail elsewhere.[37, 38] Here we will focus on the presentation of the basic concepts of each method.

5.1 Exchange spectroscopy

Exchange spectroscopy (EXSY) is one of the oldest two-dimensional NMR experiments.[39] EXSY is appropriate in the case of slow exchange with significant populations for all states. In EXSY, the magnetisation is stored along the longitudinal axis. If exchange takes place, a cross-peak correlating the chemical shifts of the two states will be observed. When this experiment is run to correlate proton chemical shifts in exchanging states, it is exactly identical to the well-known nuclear Overhauser spectroscopy (NOESY) experiment. The efficiency of NOESY in proteins and the low memory time of protons (longitudinal relaxation time) make the use of proton EXSY in protein inadequate. In the most common variant, the magnetisation is stored on nitrogen-15 nuclei during the exchange delay.[40] This experiment is most adapted when exchange rates k_{ex} are comparable to or moderately higher than longitudinal relaxation rates, thus between a fraction of 1 s^{-1} and ~50 s^{-1} (for faster processes, exchange-induced line-broadening is likely to make one or all signals invisible).

5.2 Chemical exchange saturation transfer

When line broadening precludes the observation of at least one of the exchanging states, EXSY-based techniques become impractical. Such a situation is common for exchange processes with highly skewed populations and thus a minor "invisible state" (see Figure 8.a). The next three sections will be devoted to methods designed to study such exchanging systems.

The characterization of slow chemical exchange with a state with low population can be pursued with chemical exchange saturation transfer (CEST). CEST belongs to the "family" of saturation transfer based experiments introduced in the early 60's. The principle of CEST experiments is to observe indirectly a state in exchange with an observable state. This method is particularly useful to identify invisible minor states in exchange with a major state. The magnetisation of the minor population is selectively saturated and this saturation is transferred to the major population by means of chemical exchange.

The selective saturation in a CEST experiment is achieved with a weak radiofrequency field applied to the nucleus of interest (^{15}N for instance).[41] If the *rf*-field is applied on resonance with the major state, the longitudinal magnetisation is directly saturated and decreases rapidly to zero. When the *rf*-field is on resonance with the minor state, the saturation is subsequently transferred to the exchanging state. A typical saturation profile of CEST obtained from a series of 2D spectra with various frequencies of irradiations, exhibits two drops in intensities at the resonance frequencies of the minor and major state (Figure 8). As compared to a simple spectrum of the exchanging species the saturation "signal" is boosted in the CEST experiment (Figure 8 a,d). CEST is applicable as long as the chemical system is in slow exchange, with a lower limit of exchange kinetics accessible set by the longitudinal relaxation rates of the observed nuclei, which for ^{13}C and ^{15}N in proteins are of the order of 1 s^{-1}.

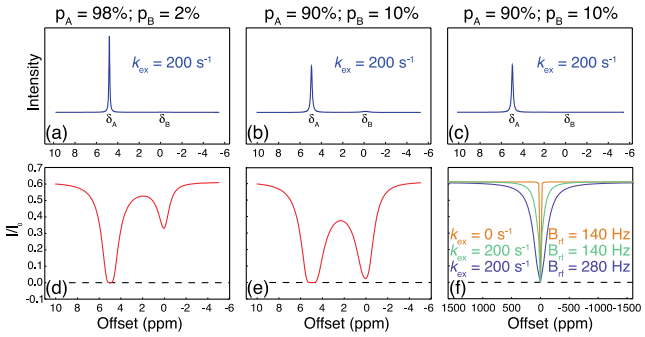

Figure 8: Principle of chemical exchange saturation transfer. (a-c) NMR spectra predicted for two-state slow exchange with skewed populations. (a) Similar intrinsic relaxation rates are used for A and B, with a low population of B, p_B = 0.02, the peak for state B cannot be observed. (b) Same as (a) with p_B = 0.1, a broad peak is seen for state B. (c) with very fast relaxation in state B (*e.g.* because state B is a very slow tumbling species) the peak for B disappears. (d-f) CEST/DEST saturation profiles. (d) Same parameters as (a), a dip in the saturation profile at the resonance frequency of "invisible" site B is observed. (e) Same parameters as (b), the second dip is very pronounced. (f) Same parameters as (c), with relaxation rates in state B characteristic of a large oligomer, a single and very broad dip in visible in the saturation profile (note the different scale on the x axis).

The minor state identified by CEST experiment can be invisible because of line broadening due to chemical exchange or extreme line broadening, as encountered in large particles or solids. In the latter case, such a "dark" state can nevertheless be identified in dark-state exchange saturation transfer (DEST) experiments. The major difference of DEST and CEST experiments is that the saturation "spectrum" of minor species derived from DEST experiments is characterized by very broad lines dominated by extremely fast relaxation. Thus the chemical shift information of the nuclei in the "dark" state is lost (Figure 8 c,f). This method was successfully applied to the study of exchange of the Aβ peptide between the small monomeric form and large oligomers.[42]

5.3 Carr-Purcell-Meiboom-Gill Dispersion

Introduced by Carr and Purcell and improved by Meiboom and Gill, CPMG (Carr-Purcell-Meiboom-Gill) relaxation dispersion is one of the main techniques to quantify chemical exchange in macromolecules. Typically applied on ^{1}H, ^{15}N and ^{13}C nuclei, CPMG relaxation dispersion minimizes the effect of the exchange contribution (R_{ex}) to the transverse relaxation rates. In this technique, the relaxation of the transverse magnetisation is observed during a train of π □□□□□□ separated by delays τ_{cp} in a constant period T_{cpmg}, a series of spin echoes repeated n times: $(\tau_{cp}$-π□$\tau_{cp})_n$ where n is an integer.[37, 43] When the delay τ_{cp} is long: $\tau_{cp} > 1/k_{ex}$, the dephasing caused by exchange occurs during each delay τ_{cp}. The measured relaxation rate is barely altered by the CPMG sequence (Figure 9.b). When magnetisation is refocused much faster than the lifetime of the system in each state: $\tau_{cp} << 1/k_{ex}$, chemical shift evolution is suppressed for each state by a series of short echoes (Figure 9.f). Chemical exchange does not lead to any additional contribution to transverse relaxation. The relaxation rate becomes the population-weighted average of the intrinsic transverse relaxation rates in all exchanging states. The transition between the two limiting cases (Figure 9.c-e) provides quantitative information about the exchanging process. Practically, the effective relaxation rates ($R_{2,eff}$) are measured at various delays τ_{cp} leading to a dispersion curve (Figure 9.g). Information about kinetic processes is obtained by fitting dispersion curves using theoretical expressions of two- or three-site exchange. CPMG relaxation dispersion is possibly the most widely used method to characterize chemical exchange processes in proteins. The

experiment is quite robust and not very difficult to set up. CPMG relaxation dispersion experiments are limited to exchange rates ranging from ~ 50 to 2000 s^{-1}.

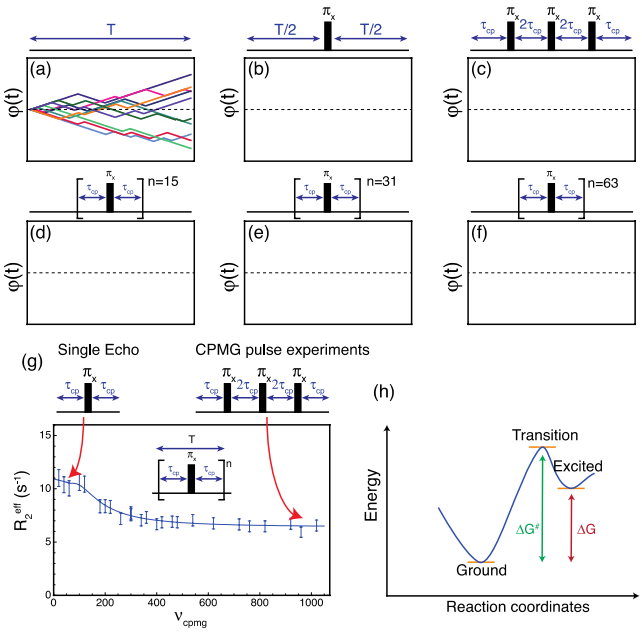

Figure 9: Evolution of the transverse magnetisation in the presence of chemical exchange for a two-site exchange A (ω_A) and B (ω_B). (a) Due to the presence of chemical exchange, the precession frequency jumps between the frequencies of state A (ω_A) and state B (ω_B). We show trajectories for ten molecules (see Figure 7 above). (b) A single spin echo, with a π-pulse applied in the middle of delay T is unable to refocus the broadening due to chemical exchange. (c-d-e-f) The application of successively increasing numbers of π-pulses during the constant period T, reduces the effects of chemical exchange. (g) An example of a CPMG relaxation dispersion profile. (h) In favourable cases the analysis of relaxation dispersion profiles provides both the activation and the Gibbs free energy of the reaction.

Experimental investigations of CPMG relaxation dispersion have been widely used to study ligand or protein binding,[44] conformational exchange, enzyme catalysis[45] or protein folding. These experiments provide information not only about kinetics but also about the chemical shifts of exchanging species. This chemical shift information can be used to calculate the structure of "invisible" excited states that cannot be directly observable in NMR spectra (e.g. the signal of site B in Figure 8.a).[46]

5.4 Relaxation in the rotating frame

A second technique commonly used to study exchange processes through the measurement of relaxation dispersion is the measurement of relaxation rates in the rotating-frame ($R_1\rho$) in the presence of an effective spin-lock *rf*-field.[47] In an $R_1\rho$ experiment, a continuous-wave radiofrequency (rf) field is applied. In the rotating frame, the magnetisation is locked along an effective field, sum of the rf field and frequency offset (see Figure 10). The $R_1\rho$ relaxation rate depends on longitudinal (R_1) and transverse (R_2) relaxation rates, and on the tilt angle θ between the effective field and the z axis.[15] In the presence of exchange, the $R_1\rho$ rate is also dependent on the amplitude of the effective field (ω_e).[15, 47]

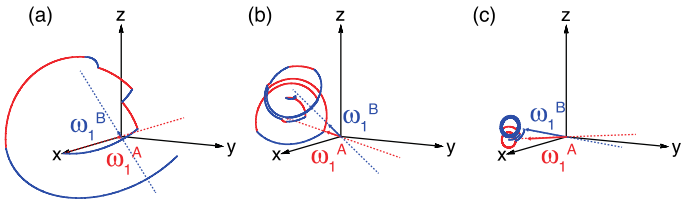

Figure 10: Evolution the magnetisation during an $R_1\rho$ experiment. The effective magnetic fields are represented as solid arrows and their directions are identified by dashed lines. (a) A weak radiofrequency field is applied on resonance with the major state A. Jumps between states lead to large variations of the rotation axis and a divergent trajectory of the magnetisation: the ensemble magnetisation along the effective field of the major state will decay fast. (b) increasing the amplitude of the effective field, the change of orientation between the two exchanging states is reduced. (c) The decay of the magnetisation aligned with the effective field becomes negligible when the effective field is large enough.

Figure 10 shows a series of trajectories of magnetisation during an $R_1\rho$ experiment in the case of slow chemical exchange. The magnetisation is initially aligned with the effective field corresponding to the ground, most populated state A. When exchange takes place, the offset component of the field changes by the difference of chemical shifts between the two states.

The tilt angle of the effective field θ changes and the magnetisation is not aligned any more with the effective field. Thus, the magnetisation starts a precession around this new effective field. A series of exchange steps back and forth, makes the magnetisation move away from the initial effective field in a stochastic way. When an ensemble average is considered, the magnetisation of the whole sample, aligned with the effective field, is progressively lost: chemical exchange leads to $R_1\rho$ relaxation. If the effective field is increased, by an increase of the offset, the rf field amplitude or both, the change of effective field and tilt angle due to the jump between the two exchanging states becomes smaller (Figure 10-b). Thus, increasing the effective field progressively quenches $R_1\rho$ relaxation due to the exchange process. In the limit of a large effective field, the relaxation rate becomes the population-weighted average of the $R_1\rho$ relaxation rates in all exchanging states. The parameters of the exchange process can be extracted from the relaxation dispersion curve showing $R_1\rho$ as a function of the effective field.

Due to the larger effective field amplitude achievable in $R_1\rho$ experiments, this technique is applicable to the study of millisecond[48] down to microsecond exchange processes. The current record is 3.4 μs.[49] This method has been successfully applied to characterize internal motions in proteins,[48] protein folding equilibrium, or ligand binding.[50]

For both CPMG and $R_1\rho$ relaxation dispersion s, the acquisition at more than one magnetic field largely improves the accuracy and the robustness of the extracted dynamic parameters.

6 Timescales and populations

As shown here, nuclear spin relaxation is sensitive to protein motions in many different ways over timescales ranging from tens of picoseconds to seconds. When proteins are in solution, reorientational motions from ~10 ps to ~10 ns can be studied by transverse and longitudinal relaxation measurements; motions from ~5 μs to ~1 s can be studied by the characterization of chemical exchange-induced relaxation. Relaxation measurements for proteins in solids (crystals, precipitates, large assemblies) or for immobilized proteins can probe reorientational motions on timescales ranging from ~10 ps to ~100 μs (in favourable cases).[21]

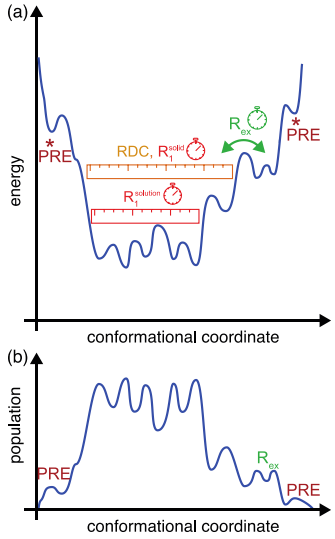

Figure 11: Schematic representation of the exploration of the conformational space of a protein. The type of motion explored by each nuclear spin relaxation-based is indicated. (a) On the energy graph, a stopwatch indicates that a method provides the timescale of a given dynamic process. Methods shown on the population graph (b) can access to populations of high-energy states.

Although timescales are important, one should be aware of what a given technique can measure and what type of motion is likely or not to be identified with a specific approach. In the simple case of a "single-well energy profile", the slower a motion, the higher the energy reached during the process and the less populated is the state explored. For instance, longitudinal relaxation rates measured on proteins in isotropic liquids provide order parameters, which are closely related to an average of accessible orientations, with decreasing weight as motions become slower than overall tumbling. The analysis of these relaxation rates will provide a solid estimate of the width of the well of the ground state on the energy surface, in quite a similar fashion as the analysis of residual dipolar couplings (see Figure 11). However, both measures will be insensitive to the presence of weakly populated states.

Other rates show enhanced sensitivity when the correlation time of a given motion increases. For instance, transverse and longitudinal relaxation rates, as measured in solids or immobilized proteins, are highly sensitive to motions on high nanosecond (see Figure 3) and micro-second timescales: the sensitive variation of the spectral density function at low frequency largely compensates the low occurrence of such slow motions.

Transverse relaxation rates are extremely sensitive to the modulation of chemical shifts by chemical exchange on timescales from microseconds to about 100 ms. However, the study of this effect is only practical when the populations of the states in

exchange are skewed, with a dominant ground state. Indeed, the exploration of exchange processes with significant populations of at least two exchanging states is usually prohibited, as the extremely high contributions of chemical exchange to line widths will prevent recording NMR spectra. The only exception to this rule is the case of very slow exchange, when exchanging states are both observable and exchange spectroscopy can be used.

Paramagnetic relaxation enhancements are due to the strong interaction between a nucleus and an electron. Thus, extremely sparse populations can be probed as long as they correspond to an event when the electron and the nucleus are in close proximity. Such rare events, such as the formation of encounter complexes or a contact between two regions of an IDP, may correspond to very sparse populations.

Note that the states identified here by a simplistic one-dimension of conformation coordinate often correspond to ensembles of microstates in exchange with one another. For instance, the states identified by chemical exchange techniques or PREs are not static but dynamic on faster timescales.

Conclusions

We have presented and discussed the broad landscape of nuclear magnetic relaxation measurements that can be used to probe dynamic processes in proteins, from picosecond librations to chemical reactions taking place on up to second timescales. These techniques offer a distinctive view on protein properties far from the static images that represent model structures derived from X-ray diffraction, cryo-electron microscopy or NMR. Essentially, nuclear magnetic relaxation approaches provide an impressive breadth of experimental observables, with atomic resolution, covering about 12 orders of magnitude of timescales of motions that will be essential for the understanding and prediction of physical and chemical properties of proteins.

Acknowledgments

We thank Ching-Yu Chou (ENS) for discussions, Pavel Kadeřávek and Guillaume Bouvignies (ENS) for assistance in preparing Figures; as well as Nicolas Bolik-Coulon, Emmanuelle Weber and Guillaume Bouvignies (ENS) for their careful reading of the manuscript. Part of the work presented here has received funding from the European Research Council (ERC) under the European Communitys Seventh Framework Programme (FP7/2007–2013), ERC Grant Agreement 279519 (2F4BIODYN).

Notes and references

[a] *École Normale Supérieure-PSL Research University, Département de Chimie, 24, rue Lhomond, 75005 Paris, France.*
Fabien.Ferrage@ens.fr
[b] *Sorbonne Universités, UPMC Univ Paris 06, LBM, 4 place Jussieu, F-75005, Paris, France.*
[c] *CNRS, UMR 7203 LBM, F-75005, Paris, France.*

† Electronic Supplementary Information (ESI) available: expressions and tables of parameters used for figures 2, 3, and 8. See DOI: 10.1039/b000000x/

‡ These authors contributed equally.

1. M. H. Levitt, *Spin Dynamics: Basics of Nuclear Magnetic Resonance*, 2nd Edition edn., John Wiley & Sons, Chichester, 2008.
2. D. Neuhaus and M. P. Williamson, *The Nuclear Overhauser Effect in Structural and Conformational Analysis*, 2nd edn., John Wiley & Sons, New York, 2000.
3. O. Millet, D. R. Muhandiram, N. R. Skrynnikov and L. E. Kay, *J. Am. Chem. Soc.*, 2002, **124**, 6439-6448.
4. V. Calandrini, D. Abergel and G. R. Kneller, *J. Chem. Phys.*, 2010, **133**.
5. G. Lipari and A. Szabo, *J. Am. Chem. Soc.*, 1982, **104**, 4546-4559.
6. B. Halle, *J. Chem. Phys.*, 2009, **131**.
7. S. F. Lienin, T. Bremi, B. Brutscher, R. Brüschweiler and R. R. Ernst, *J. Am. Chem. Soc.*, 1998, **120**, 9870-9879.
8. G. M. Clore, A. Szabo, A. Bax, L. E. Kay, P. C. Driscoll and A. M. Gronenborn, *J. Am. Chem. Soc.*, 1990, **112**, 4989-4991.
9. A. V. Buevich and J. Baum, *J. Am. Chem. Soc.*, 1999, **121**, 8671-8672.
10. V. Tugarinov, Z. C. Liang, Y. E. Shapiro, J. H. Freed and E. Meirovitch, *J. Am. Chem. Soc.*, 2001, **123**, 3055-3063.
11. S. N. Khan, C. Charlier, R. Augustyniak, N. Salvi, V. Déjean, G. Bodenhausen, O. Lequin, P. Pelupessy and F. Ferrage, *Biophys. J.*, 2015, **109**, 988.
12. B. Brutscher, R. Brüschweiler and R. R. Ernst, *Biochemistry*, 1997, **36**, 13043-13053.
13. A. M. Mandel, M. Akke and A. G. Palmer III, *J. Mol. Biol.*, 1995, **246**, 144-163.
14. J. W. Peng and G. Wagner, *J. Magn. Reson.*, 1992, **98**, 308-332.
15. A. Abragam, *Principles of Nuclear Magnetism*, Oxford University Press, Oxford, 1961.
16. N. A. Farrow, O. W. Zhang, A. Szabo, D. A. Torchia and L. E. Kay, *J. Biomol. NMR*, 1995, **6**, 153-162.
17. C. Charlier, S. N. Khan, T. Marquardsen, P. Pelupessy, V. Reiss, D. Sakellariou, G. Bodenhausen, F. Engelke and F. Ferrage, *J. Am. Chem. Soc.*, 2013, **135**, 18665-18672.
18. R. Kimmich and E. Anoardo, *Prog. Nucl. Magn. Reson. Spectrosc.*, 2004, **44**, 257-320.
19. G. Parigi, N. Rezaei-Ghaleh, A. Giachetti, S. Becker, C. Fernandez, M. Blackledge, C. Griesinger, M. Zweckstetter and C. Luchinat, *J. Am. Chem. Soc.*, 2014, **136**, 16201-16209.
20. J. P. Korb and R. G. Bryant, *J. Chem. Phys.*, 2001, **115**, 10964-10974.
21. E. Persson and B. Halle, *J. Am. Chem. Soc.*, 2008, **130**, 1774-1787.
22. A. G. Redfield, *J. Biomol. NMR*, 2012, **52**, 159-177.
23. M. W. Clarkson, M. Lei, E. Z. Eisenmesser, W. Labeikovsky, A. Redfield and D. Kern, *J. Biomol. NMR*, 2009, **45**, 217-225.
24. J. D. Haller and P. Schanda, *J. Biomol. NMR*, 2013, **57**, 263-280.
25. J. R. Lewandowski, M. E. Halse, M. Blackledge and L. Emsley, *Science*, 2015, **348**, 578-581.

26. L. P. Hwang and J. H. Freed, *J. Chem. Phys.*, 1975, **63**, 4017-4025.
27. G. M. Clore and J. Iwahara, *Chem. Rev.*, 2009, **109**, 4108-4139.
28. Y. Xue, I. S. Podkorytov, D. K. Rao, N. Benjamin, H. L. Sun and N. R. Skrynnikov, *Protein Sci.*, 2009, **18**, 1401-1424.
29. M. R. Jensen, M. Zweckstetter, J.-R. Huang and M. Blackledge, *Chem. Rev.*, 2014, **114**, 6632-6660.
30. X. Xu, W. Reinle, F. Hannemann, P. V. Konarev, D. I. Svergun, R. Bernhardt and M. Ubbink, *J. Am. Chem. Soc.*, 2008, **130**, 6395-6403.
31. J. R. Gillespie and D. Shortle, *J. Mol. Biol.*, 1997, **268**, 158-169.
32. D. F. Hansen, P. Vallurupalli, P. Lundstrom, P. Neudecker and L. E. Kay, *J. Am. Chem. Soc.*, 2008, **130**, 2667-2675.
33. T. Segawa, F. Kateb, L. Duma, P. Bodenhausen and P. Pelupessy, *ChemBioChem*, 2008, **9**, 537-542.
34. J. D. Formankay, G. M. Clore and A. M. Gronenborn, *Biochemistry*, 1992, **31**, 3442-3452.
35. I. Andre, S. Linse and F. A. A. Mulder, *J. Am. Chem. Soc.*, 2007, **129**, 15805-15813.
36. J. Wallerstein, U. Weininger, M. A. I. Khan, S. Linse and M. Akke, *J. Am. Chem. Soc.*, 2015.
37. A. G. Palmer, *Chem. Rev.*, 2004, **104**, 3623-3640.
38. A. G. Palmer and F. Massi, *Chem. Rev.*, 2006, **106**, 1700-1719.
39. B. H. Meier and R. R. Ernst, *J. Am. Chem. Soc.*, 1979, **101**, 6441-6442.
40. N. A. Farrow, R. Muhandiram, A. U. Singer, S. M. Pascal, C. M. Kay, G. Gish, S. E. Shoelson, T. Pawson, J. D. Forman-Kay and L. E. Kay, *Biochemistry*, 1994, **33**, 5984-6003.
41. P. Vallurupalli, G. Bouvignies and L. E. Kay, *J. Am. Chem. Soc.*, 2012, **134**, 8148-8161.
42. N. L. Fawzi, J. Ying, R. Ghirlando, D. A. Torchia and G. M. Clore, *Nature*, 2011, **480**, 268-U161.
43. J. P. Loria, M. Rance and A. G. Palmer, *J. Am. Chem. Soc.*, 1999, **121**, 2331-2332.
44. R. Schneider, D. Maurin, G. Communie, J. Kragelj, D. F. Hansen, R. W. H. Ruigrok, M. R. Jensen and M. Blackledge, *J. Am. Chem. Soc.*, 2015, **137**, 1220-1229.
45. E. Z. Eisenmesser, O. Millet, W. Labeikovsky, D. M. Korzhnev, M. Wolf-Watz, D. A. Bosco, J. J. Skalisky, L. E. Kay and D. Kern, *Nature*, 2005, **438**, 117-121.
46. G. Bouvignies, P. Vallurupalli, D. F. Hansen, B. E. Correia, O. Lange, A. Bah, R. M. Vernon, F. W. Dahlquist, D. Baker and L. E. Kay, *Nature*, 2011, **477**, 111-U134.
47. C. Deverell, R. E. Morgan and J. H. Strange, *Mol. Phys.*, 1970, **18**, 553-&.
48. F. Massi, E. Johnson, C. Wang, M. Rance and A. G. Palmer, *J. Am. Chem. Soc.*, 2004, **126**, 2247-2256.
49. C. A. Smith, D. Ban, S. Pratihar, K. Giller, C. Schwiegk, B. L. de Groot, S. Becker, C. Griesinger and D. Lee, *Angew. Chem.-Int. Edit.*, 2015, **54**, 207-210.
50. D. G. Davis, M. E. Perlman and R. E. London, *J. Magn. Reson., Ser B*, 1994, **104**, 266-275.